ResearchGate

See discussions, stats, and author profiles for this publication at: https://www.researchgate.net/publication/231211154

# Self-Assembled Monolayer Mechanism for Corrosion Inhibition of Iron by Imidazolines

**ARTICLE** *in* LANGMUIR · DECEMBER 1996

Impact Factor: 4.46 · DOI: 10.1021/la960646y

CITATIONS
116

READS
223

**6 AUTHORS**, INCLUDING:

Mario Blanco
King Abdullah University of Science and Tech…
**64** PUBLICATIONS **1,701** CITATIONS
SEE PROFILE

William A. Goddard
California Institute of Technology
**1,332** PUBLICATIONS **68,116** CITATIONS
SEE PROFILE

Available from: Mario Blanco
Retrieved on: 23 January 2016

# Self-Assembled Monolayer Mechanism for Corrosion Inhibition of Iron by Imidazolines

Sunder Ramachandran,[†,‡] Bao-Liang Tsai,[†] Mario Blanco,[†] Huey Chen,[§] Yongchun Tang,[§] and William A. Goddard, III*,[†]

*Materials and Process Simulation Center, Beckman Institute (139-74), Division of Chemistry and Chemical Engineering, California Institute of Technology, Pasadena, California 91125, and Chevron Petroleum Technology Company, 1300 Beach Boulevard, La Habra, California 90631*

*Received June 27, 1996*[⊗]

Some of the most effective corrosion inhibitors for oil field pipeline applications are the oleic imidazoline (OI) class of molecules. However, the mechanism by which OIs inhibit corrosion is not known. We report atomistic simulations (quantum mechanics and molecular dynamics) designed to elucidate this mechanism. These studies lead to the self-assembled monolayer (SAM) model for corrosion inhibition, which explains the differences in corrosion inhibition efficiency for various OI molecules. The SAM model of OI inhibitors involves the following critical elements: (i) The function of the OI is to form a self-assembled monolayer on the native oxide surface of iron; this serves a protective role by forming a hydrophobic barrier preventing migration of $H_2O$, $O_2$, and electrons to the Fe surface. (ii) The imidazoline head group serves as a sufficiently strong Lewis base to displace $H_2O$ from the Lewis acid sites of the iron oxide surface. (iii) These head groups self-assemble on the surface to form an ordered monolayer on the iron oxide surface. [$\sqrt{3} \times \sqrt{3}$ for the (001) cleavage surface of $\alpha$-$Fe_2O_3$.] (iv) The long hydrophobic tail (e.g., 2-oleic acid) tilts to form a tightly packed hydrophobic monolayer. [For $\alpha$-$Fe_2O_3$(001) the tilt angle is about 72° with respect to the surface normal.] (v) This hydrocarbon tail must have a sufficient length to cover the surface. [For $\alpha$-$Fe_2O_3$-(001) the chain length must be 12 or more carbon atoms.] (vi) The hydrophobic tail and the pendent group (e.g., $-CH_2CH_2NH_2$) must lead to an octanol/water partition coefficient (log *P*) below a critical value in order to rapidly form the monolayer. This SAM model should be useful in developing both alternative environmentally benign corrosion inhibitors and higher temperature corrosion inhibitors.

## 1.0 Introduction

Corrosion in pipes, pumps, turbine blades, coolers, superheaters, reheaters, fuel cells, and exhaust systems causes enormous industrial expense due to production downtime, accidental injuries, and replacement costs.[1] The cost to U.S. industry from corrosion exceeds $10 billion per year.[1] Indeed, the market for corrosion inhibitors (CIs) in the U.S. is expected to increase to $7.1 billion per year by the year 2000.[2] Most CI impose a toxic burden on the environment, making it critical to find environmentally neutral but efficient replacements.[3]

The major impediment to designing new inhibitors is that *the mechanism by which these chemical compounds prevent corrosion is not understood*.[3] The importance of determining the mechanism is illustrated by the strong dependence of efficiency upon minor changes in the chemical structure of these compounds.[3] Experimental evidence in support of specific mechanisms has been difficult to obtain due to the following: (i) the low concentrations at which these inhibitors are used (a few ppm), (ii) the complexity of the environments surrounding the inhibitor under real conditions (high temperatures and pressure and oil and/or water at high ionic strengths), and (iii) the difficulty in experimentally obtaining atomistic information about the fluid/metal interface.

Herein we report a variety of atomistic theoretical studies on oleic imidazoline (OI) inhibitors and comparisons of the studies with experimentally observed efficiencies to develop a new mechanism of corrosion inhibition for these systems. This self-assembled monolayer (SAM) mechanism suggests the following essential features for corrosion inhibitors: (i) strong bonding of the head group to Lewis acid sites on the iron oxide surface, (ii) self-assembly of the inhibitors on these surfaces to obtain a pattern controlled by the shape of the head group, (iii) self-organization of the tails to form a coherent hydrophobic film that serves as a barrier for migration of water, oxygen, and electrons to the metal surface, and (iv) optimal oil/water partitioning of the inhibitor molecules so that a monolayer can be formed on the surface with only ppm concentration in solution.

Section 2 describes the characteristics of OI molecules and some of the experiments. Section 3 describes the theoretical results on OI/surface interactions of the SAM model. Section 4 develops quantitative predictions for corrosion inhibition based upon the SAM model. Some additional discussion of the SAM model is in section 5.

## 2.0 Experimental Observations Concerning Inhibition by OI of Corrosion on Iron

Oleic imidazolines (OIs) are used extensively as inhibitors of iron corrosion in acidic media, particularly in oil field applications. As shown in Figure 1, these OI molecules consist of the following: (i) an imidazoline head group, (ii) a long hydrocarbon tail group, and (iii) a short pendent group.

In this paper we will use the following notation:

$$\text{OI}-\text{h}-\text{p}$$

where *h* indicates the hydrophobic tail and p indicates the pendent group. Examples are

* To whom correspondence should be addressed. Telefax: 818-585-0918. Phone: 818-395-2731. E-mail: wag@wag.caltech.edu, copy to debi@wag.caltech.edu.

† Beckman Institute.

‡ Current address: Baker Performance Chemicals, Inc., 3900 Essex Lane, 3rd Floor, Houston, TX 77027.

§ Chevron Petroleum Technology Co.

⊗ Abstract published in *Advance ACS Abstracts,* December 1, 1996.

(1) Zanneti, R. *Chem. Eng. (NY)* **1990**, *97*(10), 5.

(2) Hairston, D. W. *Chem. Eng. (NY)* **1996**, *103*(3), 65.

(3) Edwards, A.; Osborne, C.; Webster, S.; Klenerman, D.; Joseph, M.; Ostovar, P.; Doyle, M. *Corros. Sci.* **1994**, *36*, 315.

S0743-7463(96)00646-4 CCC: $12.00 © 1996 American Chemical Society

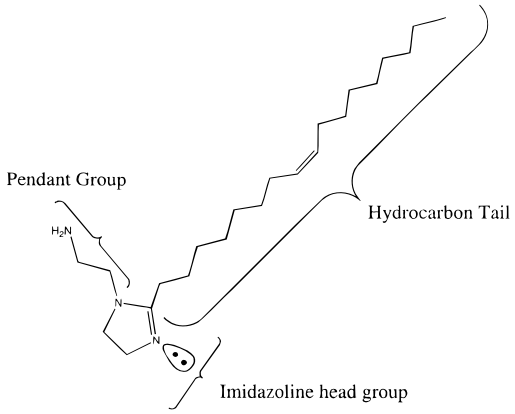


**Figure 1.** Typical OI molecule. The case shown is OI−17-(8═9)−CCN with the 1-aminoethyl pendent group and the 2-oleyl hydrophobic tail.

$$h = 15 \text{ implies } -(CH_2)_{14}CH_3 \quad (1)$$

$$h = 17(8{=}9) \text{ implies } -(CH_2)_7CH{=}CH(CH_2)_7CH_3$$

$$h = 17(8{:}OH) \text{ implies } -(CH_2)_7CH(OH)(CH_2)_8CH_3$$

etc., while

$$p = CCN \text{ implies } -CH_2CH_2NH_2 \quad (2)$$

$$p = CCO \text{ implies } -CH_2CH_2OH$$

$$p = C \text{ implies } -CH_3$$

$$p = H \text{ implies } -H$$

The oil field pipeline applications involve brines saturated with carbon dioxide, leading to a pH in the range of 4−6, depending upon the partial pressure of carbon dioxide. At anodic areas iron dissolves by (3).[4] This

$$Fe \rightleftharpoons Fe^{2+} + 2e^- \quad (3)$$

reaction is rapid in most media.[4]

In deaerated solutions the cathodic reaction is given by (4). This reaction proceeds rapidly in acids but only slowly

$$2H^+ + 2e^- \rightleftharpoons H_2 \quad (4)$$

in alkaline or neutral media. The cathodic reaction is accelerated by dissolved oxygen in accord with the depolarization reaction (5).[4] Depending upon conditions,

$$O_2 + 4H^+ + 4e^- \rightleftharpoons 2H_2O \quad (5)$$

various Fe-containing products may form including ferrous hydroxide [$Fe(OH)_2$] or hydrous ferrous oxide ($FeO{\cdot}nH_2O$) which may be converted to hydrous ferric oxide or ferrous hydroxide.[4,5]

Analysis[6] of the adherent corrosion product reveals the presence of hematite $\alpha$-$Fe_2O_3$, nonstoichiometric magnetite $Fe_3O_4$, and lepidocrocite $\gamma$-FeOOH. Figure 2 shows a schematic representation of the aqueous corrosion of mild steel with $Fe^{2+}$ dissolving from the bare metal and reacting to form a nonpassivating porous adherent corrosion product that does not interfere with the access of electrolyte to the metal surface.[5]

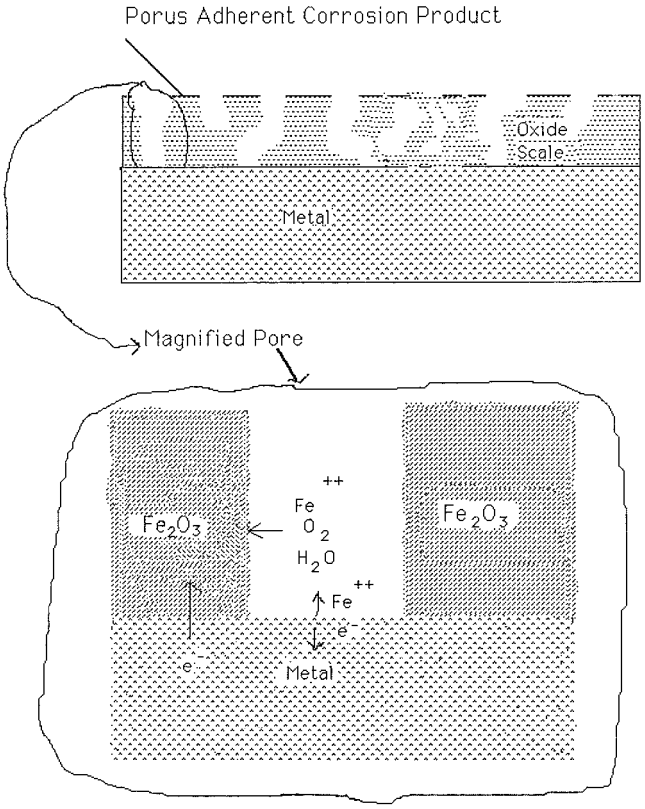


**Figure 2.** Sketch of corroding Fe surface.

McMahon[7] performed partitioning and adsorption experiments on OI−17(8═9)−CCN in an oil/water/iron system. Edwards et al.[3] measured the corrosion resistance for several OI derivatives. The adsorption of OI−17(8═9)−CCN onto mild steel has been studied using second-harmonic generation.[8,9] and sum-frequency generation techniques.[10] Pebere et al.[11] have measured the corrosion inhibition and critical micellar concentrations (cmc) of OI−16 and of 2-hexadecylimidazole.

The observed percentage corrosion inhibition efficiency[3,12] (CIE) for various OIs is listed in Table 1, which shows variations in CIE from 13% to 99%. The CIE is defined in terms of weight loss.

### 3.0 OI−Surface Interactions

**3.1 Iron Surface.** Hydrous ferric oxide, which has an orange to red-brown color, comprises most of ordinary rust. It exists as nonmagnetic $\alpha$-$Fe_2O_3$ (hematite) or as magnetic $\gamma$-$Fe_2O_3$ (maghemite), with the $\alpha$ form more stable.[4] As iron cools from 1000 to 250° it oxidizes to form an outmost oxide layer of hematite[5] $\alpha$-$Fe_2O_3$. At pH 4−5 (and electrode potentials above 0.0−0.2), the stable oxide is[4,5] $\alpha$-$Fe_2O_3$ (hematite). In operation the pH in oil/water mixtures in pipelines tends to be 4.5, suggesting $\alpha$-$Fe_2O_3$ as the dominant oxide on the Fe surface.

We assume that manufacturing and laying a pipeline made of mild steel leads to a similar hematite nonpassivating oxide film on the Fe surface. We assume that the function of the OI is to stabilize this layer against

(4) Uhlig, H. H.; Revie, R. W. *Corrosion and Corrosion Control*, 3rd ed.; John Wiley and Sons: New York, 1985.
(5) Scully, J. C. *The Fundamentals of Corrosion*, 3rd ed.; Pergamon Press: Oxford, U.K. **1990**.
(6) Kallay, N.; Kovacevic, D.; Dedic, I.; Tomasic, V. *Corrosion (Houston)* **1994**, *50*, 598. Herrera, V.; Hernandez, D. *Hyperfine Interact.* **1991**, *67*, 575. Wolski, W.; *Corrosion (Houston)* **1990**, *46*, 743.
(7) McMahon, A. J. *Colloids Surf. A* **1991**, *59*, 187.
(8) Joseph, M.; Hodge, J.; Klenerman, D. *Faraday Discuss.* **1992**, *94*, 273.
(9) Joseph, M.; Klenerman, D. *J. Electroanal. Chem.* **1992**, *340*, 301.
(10) Maechling, C. R.; Kliner, D. A. V.; Klenerman, D. *Appl. Spectrosc.* **1992**, *47*, 167.
(11) Pebre, N.; Duprat, M.; Dabosi, F.; Lattes, A.; De Savignac, A. *J. Appl. Electrochem.* **1988**, *18*, 225.
(12) Chen, H. L., unpublished data.

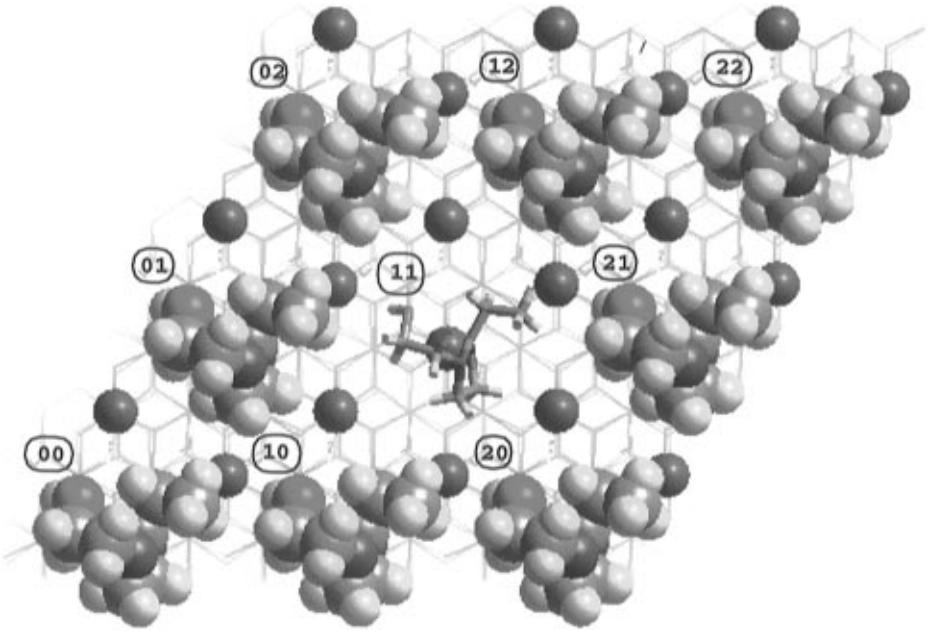


**Figure 3.** Surface structure of OI−2−CCO on hematite (α-$Fe_2O_3$). The $-C_2H_5$ hydrophobic tail is used to avoid obscuring the head group. A CPK model of the OI is used except for the molecule at the (11) site which is shown with cylinders. The surface Fe atoms are shown in black. Binding the OI to one Fe blocks binding of an OI to the six nearest neighbor Fe atoms (at 5.038 Å). The result is the $\sqrt{3} \times \sqrt{3}$ unit cell with sides of 8.736 Å. The $-CH_2CH_2OH$ pendent group is not large enough to bind with an adjacent Fe. The various cells are numbered ($n$, $m$) where $n$, $m = 0, 1, 2, ....$

**Table 1. Corrosion Inhibition of OI Molecules**

| label | pendent group | hydrophobic tail | exptl corrsn inhibition (%) |
|---|---|---|---|
| 2−CCO | $-(CH_2)_2OH$ | $CH_3(CH)_2-$ | 13[a] |
| 7−CCN | $-(CH_2)_2NH_2$ | $CH_3(CH_2)_6-$ | 17[b] |
| 8−CCN | $-(CH_2)NH_2$ | $CH_3(CH_2)_7-$ | 45[b] |
| 9−CCN | $-(CH_2)NH_2$ | $CH_3(CH_2)_8-$ | 52[b] |
| 10−CCN | $-(CH_2)NH)2$ | $CH_3(CH_2)_9-$ | 33[b] |
| 10(9=10)−CCN | $-(CH_2)_2NH_2$ | $CH_2=CH(CH_2)_8-$ | 23[b] |
| 11−CCN | $-(CH_2)_2NH_2$ | $CH_3(CH_2)_{10}$ | 77[b] |
| 12−CCN | $-(CH_2)_2NH_2$ | $CH_3(CH_2)_{11}$ | 95[b] |
| 13−CCN | $-(CH_2)_2NH_2$ | $CH_3(CH_2)_{12}-$ | 87[b] |
| 14−CCN | $-(CH_2)_2NH_2$ | $CH_3(CH_2)_{13}-$ | 82[b] |
| 15−CCN | $-(CH_2)_2NH_2$ | $CH_3(CH_2)_{14}-$ | 99[b] |
| 16−CCN | $-(CH_2)_2NH_2$ | $CH_3(CH_2)_{15}-$ | 98[b] |
| 17−CCN | $-(CH_2)_2NH_2$ | $CH_3(CH_2)_{16}-$ | 86[b] |
| 17(8=9)−CCN | $-(CH_2)_2NH_2$ | $CH_3(CH_2)_7CHCH(CH_2)_7-$ | 86−92,[b] 92[a] |
| 17(8=9)−C | $-CH_3$ | $CH_3(CH_2)_7CH=CH(CH_2)_7-$ | 90[a] |
| 17(8=9)−CCO | $-(CH_2)_2OH$ | $CH_3(CH_2)_7CH=CH(CH_2)_7-$ | 90[a] |
| 17(8=9)−CCCN | $-(CH_2)_3NH_2$ | $CH_3(CH_2)_7CH=CH(CH_2)_7-$ | 90[a] |
| 17(8≡9)−CCN | $-(CH_2)_2NH_2$ | $CH_3(CH_2)_7C\equiv C(CH_2)_7-$ | 97[b] |
| 17[11:CH(OH)−CCN | $-(CH_2)_2NH_2$ | $CH_3(CH_2)_5[CH(OH)](CH_2)_{10}-$ | 93[b] |
| 17(8=9,11=12)−CCN | $-(CH_2)_2NH_2$ | $CH_3(CH_2)_4CH=CHCH_2CH=CH(CH_2)_7-$ | 85[b] |
| 19−CCN | $-(CH_2)_2NH_2$ | $CH_3(CH_2)_{18}-$ | 85[b] |
| 21−CCN | $-(CH_2)_2NH_2$ | $CH_3(CH_2)_{20}-$ | 19.5[b] |
| 21(11=12)−CCN | $-(CH_2)_2NH_2$ | $CH_3(CH_2)_8CH=CH(CH_2)_{10}-$ | 63[b] |

[a] Reference 3. [b] Reference 12.

further oxidation. Consequently we studied how OI binds to the surface of $Fe_2O_3$. Our hypothesis that the OI interacts with α-$Fe_2O_3$ is supported by the work of McMahon[7] who measured the adsorption of OI−17(8=9)−CCN onto both iron and iron oxide powders and found similar adsorption isotherms and surface coverage.

To study the OI/$Fe_2O_3$ interactions, we developed the MS force field (FF)[13] to describe the bulk and surface structure of $Fe_2O_3$ and to describe the binding of OI to this surface. The MS FF suggests that the (001) surface of α-$Fe_2O_3$ is the most stable. Indeed, experiments[14] indicate that the (001) surface is most stable with little surface relaxation from the bulk structure.

The surface Fe of $Fe_2O_3$ will be missing one to three of its normal six lattice oxygen ligands. In aqueous media, we expect the missing sites to be replaced by $OH^-$ or $H_2O$ from the solvent. The ratio of $OH^-$ to $H_2O$ on the surface will be determined by the pH, by the surface plane of $Fe_2O_3$, and by the relative energetics. We find[13] that the OI bonds strongly as a Lewis base to $Fe^{3+}$, and we assume that on the surface of $Fe_2O_3$ it displaces one to two surface $H_2O$s.

**3.2 OI Head Group.** Two factors dictate the coverage of OI on the surface: (i) strong adsorption to the surface and (ii) the intrinsic steric bulk (the footprint) of the head group. The quantum mechanical calculations[13] indicate that OI bonds to the iron of α-$Fe_2O_3$ substantially stronger than does water. Thus OI should easily displace bound water molecules from the hematite surface. This agrees with the experimental observation (vide infra) that OI molecules absorb rapidly.

After bonding an OI to one Fe site of the (001) surface, we find that unfavorable steric interactions preclude

(13) Ramachandran, S.; Tsai, B.-L.; Blanco, M.; Chen, H.; Tang, Y.; Goddard, W. A., III. *J. Phys. Chem*., in press.
(14) Eggleston, C. M.; Hochella, M. F. *Am. Mineral* **1992**, *77*, 911.

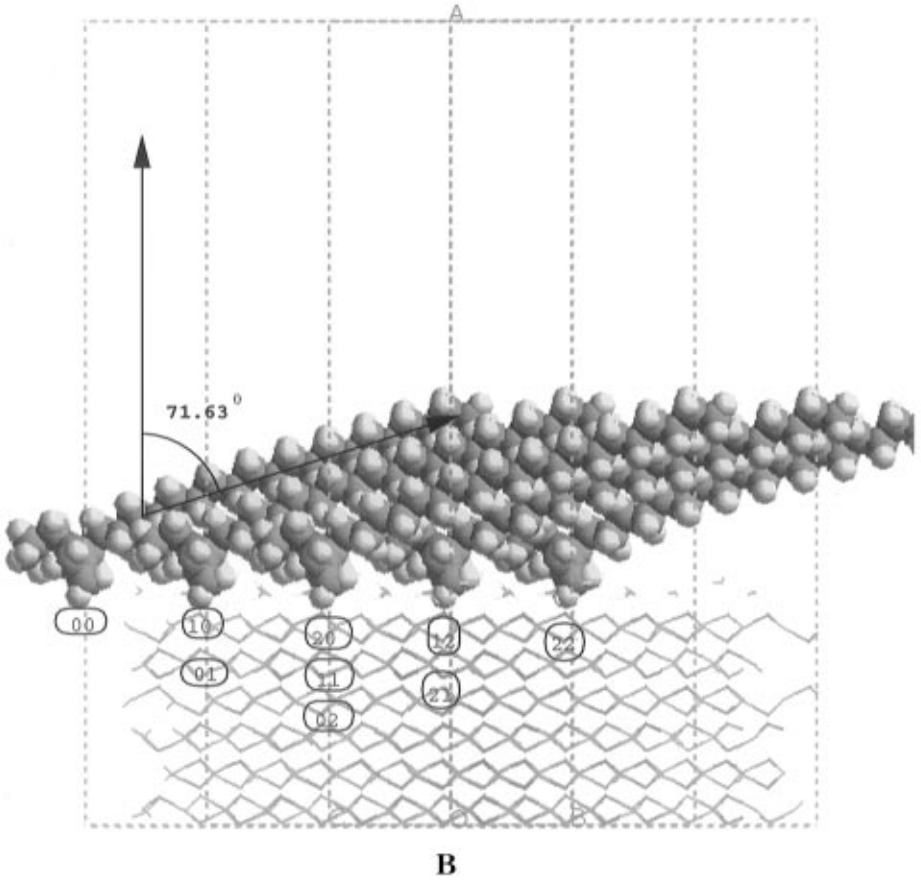


B

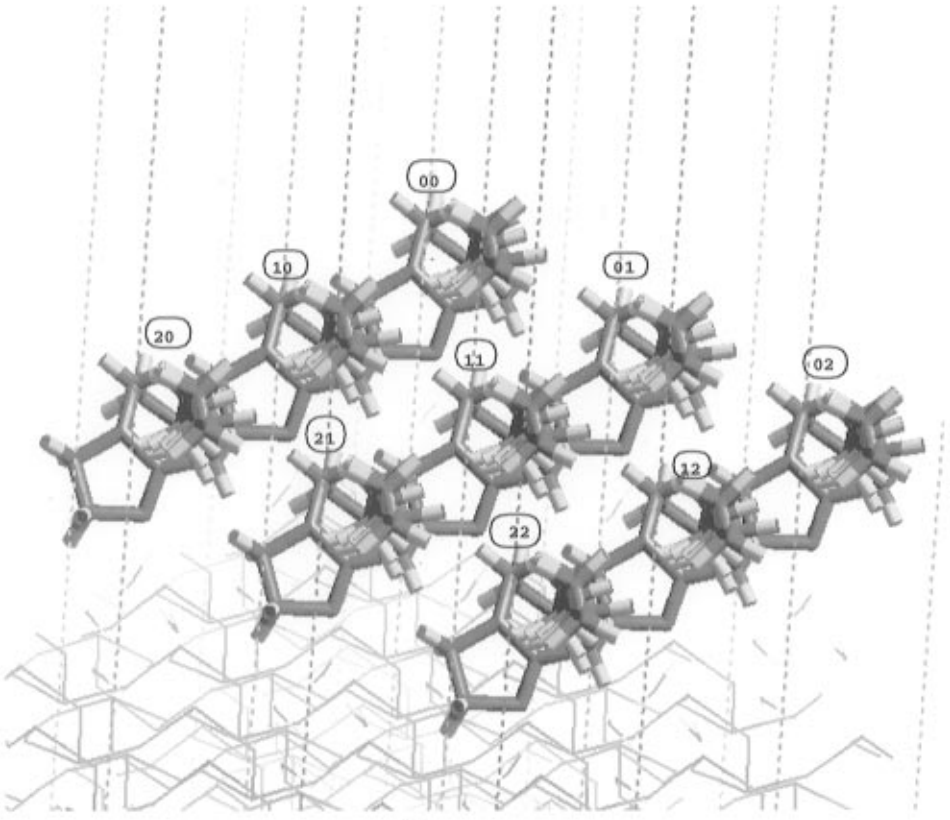


A

**Figure 4.** Optimum structure for OI−21−CCN on $Fe_2O_3$. (a) Side view: the tilt angle (defined using $C_4$ and $C_{20}$) is $\psi = 71.63°$. (b) Packing of the alkyl chains as seen from an angle parallel to the alkyl chains (71.6° from the surface normal). Focusing on the chain of cell (11), we see the closest packing with two $\gamma$ neighbors [(00) and (22)] and four $\beta$ neighbors [(10), (01), (21), and (12)].

binding a second OI to the nearest neighbor sites (at 5.038 Å). However, the footprint (steric bulk) for OI on the hematite surface is quite compatible with the second-nearest neighbor spacing of 8.726 Å. Thus the highest coverage is obtained by binding OI to next-nearest neighbor iron sites (at 8.726 Å) on the (001) surface of

hematite. This leads to the $\sqrt{3} \times \sqrt{3}$ unit cell of adsorbed OI shown in Figure 3 [for OI−2−CCO]. Thus a full monolayer of OI covers $\sigma = {}^1/_3$ of the surface Fe sites or one OI per 65.94 Å$^2$ of surface.

McMahon[7] carried out $^{14}C$ tracer studies to determine the adsorption of OI−17(8═9)−CCN onto iron and iron oxide powders. He found strong adsorption to both iron and the iron oxide surfaces, leading to saturation coverages of 65 Å$^2$ per molecule for both surfaces. This is consistent with the predicted coverage of 65.94 Å$^2$.

In the SAM model we assume that the OI self-assembles (on the $Fe_2O_3$ surface) to form a monolayer whose spacing is dictated by the size and shape of the imidazoline head group. Other molecules would lead to SAMs with different spacings depending upon their footprint and the nature of binding to iron oxide. Thus for carboxylate acids (RCOOH) and alkylamines ($RNH_2$) we find that a molecule can bind to every surface iron site, leading to $\sigma = 1$. This is expected to lead to a SAM with 21.98 Å$^2$ per molecule. Indeed, for stearic acid $C_{17}H_{35}COOH$) Xing et al.[15] found a limiting surface area of 21 Å$^2$ per molecule (from measuring the isotherm of surface pressure vs area occupied per monolayer). This agrees with the expectation of full coverage of the surface, $\sigma = 1$. For adsorption of the amines ($n$-$C_3H_7$)$NH_2$ and ($n$-$C_4H_9$)$NH_2$ from the vapor state to freshly oxidized iron, Yao[16] found surface coverages of 25−28 Å$^2$ per molecule. This indicates that primary amines cover about 80% of the iron sites on iron oxide.

These results indicate that the SAM model may be appropriate for general classes of corrosion inhibitors.

**3.3 Hydrophobic Tail. 3.3.1 Tilt Angle.** We concluded above that on the α-$Fe_2O_3$ surface of OI head groups are spaced at 8.726 Å, corresponding to second-nearest neighbor Fe atoms. For maximum coverage of the monolayers, the tails should interact with each other. In a polyethylene crystal, each chain is all-trans with four neighboring chains at 4.4 Å and two at 4.8 Å, leading to an average of 4.53 Å. To achieve strong cohesion, the tails must all be tilted with respect to the surface normal by some tilt angle $\psi$. If these tails are tilted toward the long axis of the unit cell as in Figure 4a, the tail of cell 00 will contact the tail of cell 11 when the tilt angle is

$$\cos \psi = \frac{d}{8.726\sqrt{3}} \tag{6}$$

where $d = 4.53$ Å.[17] The same tilt angle will also lead to contact between tail 00 and tails 01 and 10 (a separation of d = 4.53 Å). Equation 6 suggests a tilt angle of 72.6° with respect to the surface normal. Indeed using the MS FF we find an optimum structure for OI−21 (see Figure 4a) with $\psi = 71.6°$ (measured with respect to the line connecting $C_4$ and $C_{20}$ of the tail). Viewing this optimum structure along a line parallel to the tail (Figure 4b), we see that the alkane tails are closest packed.

Figure 5 shows a top view for the optimum structure of OI−$n$−CCN with $n = 7$, 11, and 12 carbons. With $n =$ 12 or more carbons the surface is completely covered. The fraction of the surface covered for $n < 12$ is approximately linear with $n$. Thus we define the fractional area coverage function

$$f = n/12 \text{ for } n \le 12 \tag{7a}$$

$$f = 1 \text{ for } n \ge 12 \tag{7b}$$

**3.3.2 Cohesive Energy.** Each tail has six neighbors. Thus starting with chain 11 there are tail/tail interactions with chains 12, 21, 10, and 01 for $n \ge 6$ and tail/tail interactions with chain 00 and 22 for chains $n \ge 12$. Thus for $n \ge 12$ we expect the cohesive energy within the hydrophobic film to be

$$E_{coh} = [2(n-6) + (n-12)]\left(\frac{1}{3}E_{CH_2}\right) \tag{8}$$

where $E_{CH_2} = 1.87$ kcal/mol is the cohesive energy of PE.[18] For OI−$n$−CCN we find that the cohesive energy within the hydrophobic film (see Figure 6) has the form

$$E_{coh} = \alpha \text{ for } n \le 5 \tag{9a}$$

$$E_{coh} = \alpha + 2\beta(n-5) \text{ for } 5 < n \le 11 \tag{9b}$$

$$E_{coh} = \alpha + 2\beta(n-5) + \gamma(n-11) \text{ for } n > 11 \tag{9c}$$

where $\alpha = 3.7843$, $\beta = 0.4565$, and $\gamma = 0.6196$. This bilinear behavior is expected from Figure 4b. For $n \ge 12$ each chain has six neighbors, leading to a cohesive energy increment of $\gamma + 2\beta$ for each additional carbon. Here $\gamma$ is for the two neighbors in the direction of the tilt, while $\beta$ is for the other four tail/tail interactions (we divide by two to avoid double counting). Note that $2\beta + \gamma = 1.53$ kcal/mol is close to the value of $E_{CH_2} = 1.87$ for PE.[18] For $n \le 5$ the tails are too short to interact. For the intermediate lengths only the $\beta$ neighbors interact.

**3.3.3 Entropy.** In the SAM model each alkyl chain in the monolayer is in the extended (all-trans) conformation, whereas it has a large number of favorable conformations in solution. Thus forming the film leads to a substantial decrease in entropy. Using rotational isomeric state (RIS) theory,[19] we estimate this entropy loss to be

$$\Delta S_{RIS} = -R \ln Z \tag{10}$$

where $Z$ is given by (11a). In (11a), $\beta_1$ and $\beta_2$ are the roots

$$Z = \frac{(1-\beta_2)\beta_1^{n-1} + (\beta_1 - 1)\beta_2^{n-1}}{\beta_1 - \beta_2} \tag{11a}$$

of (11b). The quantitites $\sigma_1 = 0.43$ and $\omega = 0.049$ were

$$\beta_1, \beta_2 = 1 + \sigma_1(1+\omega) \sqrt{[1-\sigma_1(1+\omega)]^2 + \frac{8\sigma_1}{2}} \tag{11b}$$

used for the calculation.[19] These values from Abe, Jernigan, and Flory[20] reproduced the experimentally obtained energy difference of 2.1 kJ/mol between trans,-gauche, and trans,trans states of $n$-pentane and 7.5 kJ/mol between (+)gauche, (−)gauche states and trans/trans states of $n$-pentane, respectively. This leads to the results for $\Delta S_{RIS}/R$ in Table 2.

Changes in the distribution of vibrational frequencies may also contribute to $\Delta S$; however, we will ignore this contribution.

**3.3.4 Observed Corrosion Inhibition.** Figure 7 shows the experimental corrosion inhibition data[12] for OI−$n$−CCN with $n = 7$−21. These experiments[12] were performed under conditions similar to (296 K) those of

(15) Xing, W.; Shan, Y.; Guo, D.; Lu, T.; Xi, S. *Corrosion (Houston)* **1995**, *51*, 45.
(16) Yao, Y. Y. *J. Phys. Chem.* **1963**, *67*, 2055.
(17) Gerdy, J. J.; Goddard, W. A., III. *J. Am. Chem. Soc.* **1996**, *118*, 3233.
(18) Karasawa, N.; Dasgupta, S.; Goddard, W. A., III. *J. Phys. Chem.* **1991**, *95*, 2260.
(19) Mattice, W. L.; Suter, U. W. *Conformation Theory of Large Molecules*; John Wiley: New York, 1994.
(20) Abe, A.; Jernigan, R. L.; Flory, P. L. *J. Am. Chem. Soc.* **1965**, *87*, 631.

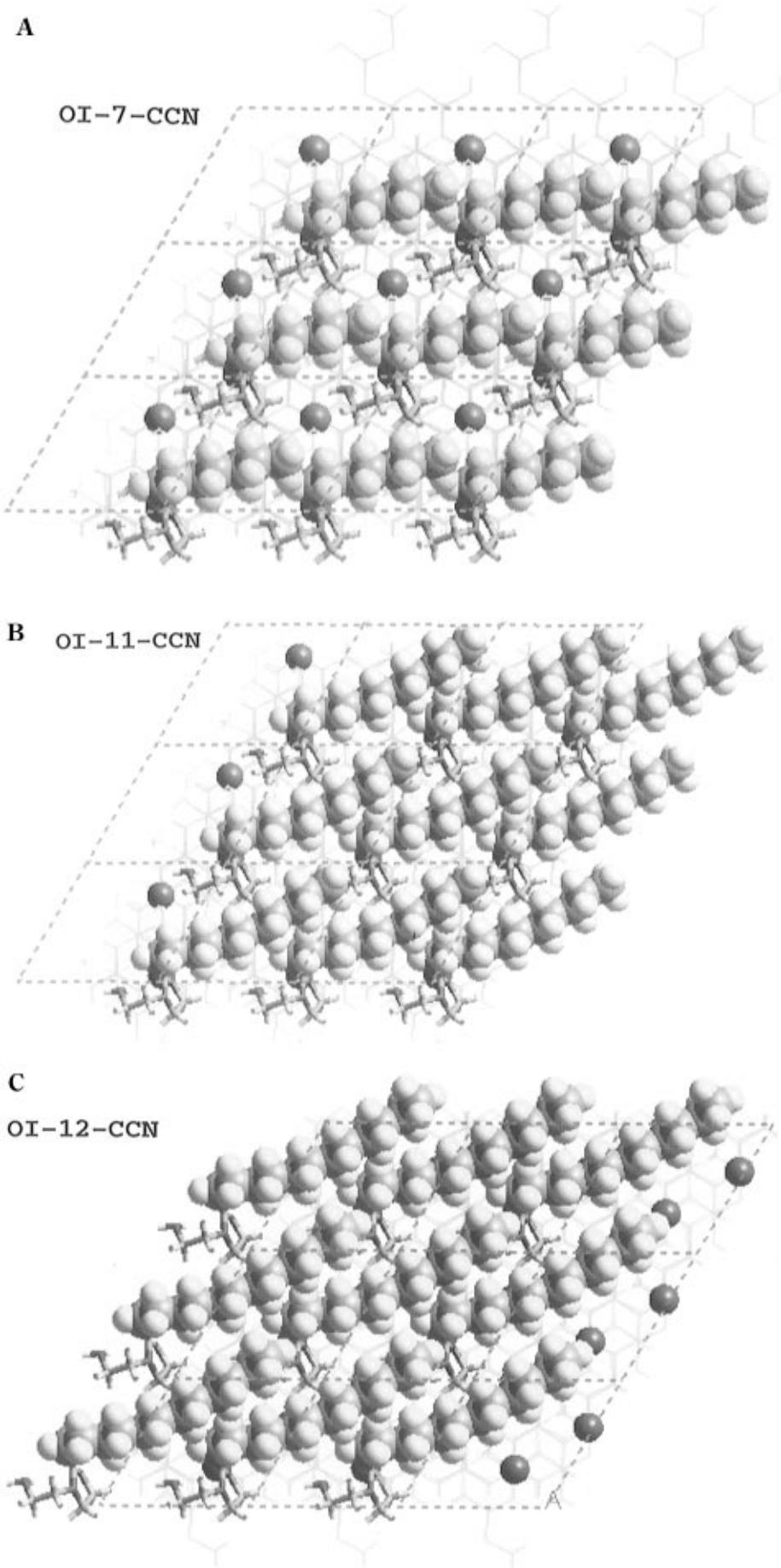


**Figure 5.** Top view of surface showing nine unit cells with one OI per unit cell: (a) OI−7−CCN (17% observed corrosion inhibition) shows considerable uncovered surface; (b) OI−11−CCN (77% observed corrosion inhibition) shows that the head group is not covered; and (c) OI−12−CCN (95% observed corrosion inhibition) shows complete coverage.

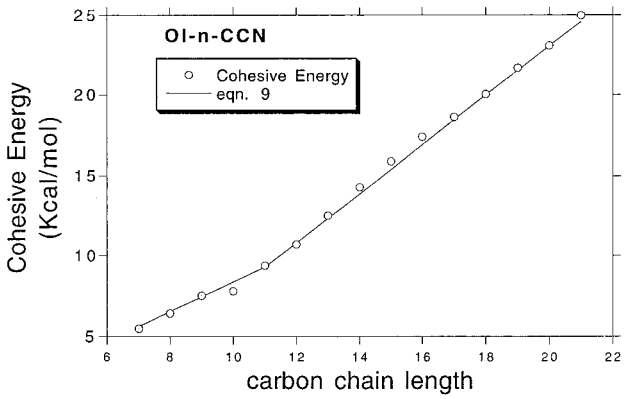


**Figure 6.** Cohesive energy predicted for OI−*n*−CCN.

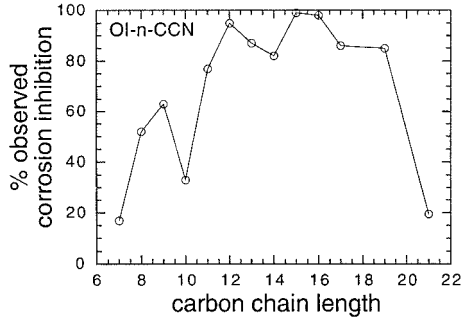


**Figure 7.** Observed experimental corrosion inhibition of OI−*n*−CCN. The data are from ref 12.

**Table 2. Cohesive Energy ($E_{coh}$ in kcal/mol), Entropy Loss ($\Delta S_{RIS}/R$), log *P*, and Fractional Occupation (*f*) Calculated for Various Imidazolines**

| pendent | *E* | $\Delta S_{RIS}/R$ | *f* | log *P* |
|---|---|---|---|---|
| 2−CCO | −0.441 | 0.0 | 0.1667 | −1.864 |
| 7−CCN | 5.48 | 2.719 | 0.583 | −0.858 |
| 8−CCN | 6.42 | 3.249 | 0.667 | 1.387 |
| 9−CCN | 7.51 | 3.788 | 0.75 | 1.916 |
| 10−CCN | 7.79 | 4.310 | 0.833 | 2.445 |
| 10(9═10)−CCN | 7.25 | 3.260 | 0.833 | 1.961 |
| 11−CCN | 9.36 | 4.848 | 0.917 | 2.974 |
| 12−CCN | 10.70 | 5.37 | 1.0 | 3.503 |
| 13−CCN | 12.51 | 5.89 | 1.0 | 4.032 |
| 14−CCN | 14.28 | 6.43 | 1.0 | 4.561 |
| 15−CCN | 15.89 | 6.95 | 1.0 | 5.070 |
| 16−CCN | 17.41 | 7.49 | 1.0 | 5.619 |
| 17−CCN | 18.61 | 8.01 | 1.0 | 6.148 |
| 17(8═9)−CCN | 12.94 | 5.97 | 1.0 | 5.664 |
| 17(8═9)−C | 10.13 | 5.97 | 1.0 | 6.127 |
| 17(8═9)−CCO | 13.92 | 5.97 | 1.0 | 5.587 |
| 17(8═9)−CCCN | 10.21 | 5.97 | 1.0 | 5.298 |
| 17(8≡9)−CCN | 17.29 | 5.97 | 1.0 | 4.790 |
| 17(11:CH(OH)−CCN | 17.11 | 8.01 | 1.0 | 4.208 |
| 17(8═9,11═12)−CCN | 12.13 | 4.39 | 1.0 | 5.180 |
| 18−CCN | 20.04 | 8.51 | 1.0 | 6.677 |
| 19−CCN | 21.68 | 9.07 | 1.0 | 7.206 |
| 20−CCN | 23.07 | 9.60 | 1.0 | 7.735 |
| 21−CCN | 24.96 | 10.12 | 1.0 | 8.264 |
| 21(11═12)−CCN | 23.68 | 7.56 | 1.0 | 7.780 |

Edwards et al.[3] Here we see that $n < 12$ leads to poor performance, consistent with the minimum length predicted by the SAM model. The corrosion inhibition efficiency at 296 K is roughly constant from $n = 12-19$ but drops markedly for $n = 21$. We will consider next the reason for the drop at $n = 21$.

## 4.0 Effect of Solubilities and Partition Coefficients on Corrosion Inhibition

In this section we consider the role of diffusion and adsorption on the inhibition of corrosion of iron by OI compounds. Relevant issues here are (a) solubility of OI in water, (b) the time scale for mass transport of sufficient

**Table 3. Predicted Corrosion Inhibition Efficiency (%) from Experiments and from Theory (for Different Temperatures). The Predictions Are Based on Table 2**

| | | predicted | | | | |
|---|---|---|---|---|---|---|
| molecule | exptl 296 K | 296 K | 300 K | 350 K | 400 K | 450 K |
| 2−CCO | 13.0[a] | 0.0 | 0.0 | 0.0 | 0.0 | 0.0 |
| 7−CCN | 17.0[b] | 35.3 | 33.5 | 15.5 | 6.9 | 3.4 |
| 8−CCN | 45.0[b] | 53.9 | 52.3 | 29.1 | 13.1 | 6.0 |
| 9−CCN | 52.0[b] | 70.3 | 69.4 | 50.4 | 26.0 | 11.7 |
| 10−CCN | 33.0[b] | 77.5 | 76.5 | 52.7 | 24.8 | 10.4 |
| 10(9═10)−CCN | 23.0[b] | 78.2 | 77.4 | 57.9 | 31.8 | 15.2 |
| 11−CCN | 77.0[b] | 90.9 | 90.7 | 82.7 | 57.7 | 28.8 |
| 12−CCN | 95.0[b] | 99.8 | 99.8 | 97.3 | 83.9 | 53.7 |
| 13−CCN | 87.0[b] | 100.0 | 100.0 | 99.6 | 96.7 | 83.4 |
| 14−CCN | 82.0[b] | 100.0 | 100.0 | 99.9 | 99.3 | 95.3 |
| 15−CCN | 99.0[b] | 100.0 | 100.0 | 100.0 | 99.8 | 98.6 |
| 16−CCN | 98.0[b] | 100.0 | 100.0 | 100.0 | 99.9 | 99.1 |
| 17−CCN | 86.0[b] | 100.0 | 100.0 | 100.0 | 99.9 | 98.7 |
| 17(8═9)−CCN | 92.0[a] | 100.0 | 100.0 | 99.5 | 94.9 | 75.2 |
| 17(8═9)−C | 90.0[a] | 94.3 | 92.9 | 53.4 | 15.6 | 4.3 |
| 17(8═9)−CCO | 90.0[a] | 100.0 | 100.0 | 99.9 | 98.7 | 91.6 |
| 17(8═9)−CCCN | 90.0[a] | 99.1 | 98.9 | 88.3 | 54.4 | 22.1 |
| 17(8≡9)−CCN | 97.0[b] | 100.0 | 100.0 | 100.0 | 100.0 | 99.9 |
| 17(11:CH(OH)−CCN | 93.0[b] | 100.0 | 100.0 | 100.0 | 99.9 | 98.9 |
| 17(8═9,11═12)−CCN | 85.0[b] | 100.0 | 100.0 | 99.8 | 98.6 | 92.6 |
| 18−CCN | | 99.8 | 99.8 | 99.8 | 99.7 | 98.3 |
| 19−CCN | 85.0[b] | 97.3 | 97.3 | 97.3 | 97.3 | 97.3 |
| 20−CCN | | 68.8 | 68.8 | 68.8 | 68.8 | 68.6 |
| 21−CCN | 19.5[b] | 13.7 | 13.7 | 13.7 | 13.7 | 13.7 |
| 21(11═12)−CCN | 63.0[b] | 60.6 | 60.6 | 60.6 | 60.6 | 60.6 |

[a] Reference 3. [b] Reference 12.

OI from the water solution to the surface, (c) the time scale for adsorption of OI into the monolayer, and (d) the time scale for rearrangement of the OI in the monolayer to form the stable coherent SAM.

Klenerman, Hodge, and Joseph[21] found that it took 30−40 min for OI−17(8═9)−CCN in water to form a monolayer on the Fe surface. In addition, McMahon[7] measured solubility and transport data of OI−17(8═9)−CCN in water and estimated that it took 15 min to transport this compound to the Fe surface. All four of the features may play a role in these observations. Each factor may depend upon the length of the hydrophobic tail, upon the character of the pendant group, and upon the kinetics of transport, adsorption, and ordering in the monolayer. To simplify our analysis we will consider only diffusive and solubility effects on the kinetic aspects of monolayer formation. We will assume that (i) the kinetic aspects of OI inhibition are dominated by diffusion to the surface, while (ii) the equilibrium aspects of monolayer formation are described by Langmuir isothermal adsorption.

**4.1 Dependence of Corrosion Efficiency on the Partition Coefficient, log *P*.** Because the OIs have hydrophobic and polar components and because they operate in systems involving mixtures of oil and water, we considered that the octanol/water partition coefficient (12) would be an important characteristic, where *c* is concentration.

$$P = \frac{c(n\text{-octanol})}{c(H_2O)} \tag{12}$$

The solubility $S_w$ of an organic liquid in water [in units of molarity (mol/L of water)] is related to *P* by (13).[22]

$$\log S_w = -\log P + 0.8 \tag{13}$$

The concentration in ppm ($c_{ppm}$) of an organic liquid in water is given by (14),where MW is the molecular weight of the compound. McMahon[7] measured the solubility of

(21) Klenerman, D.; Hodge, J.; Joseph, M. *Corros. Sci.* **1994**, *36*, 301.
(22) Yalkowsky, S. H.; Banerjee, S. *Aqueous Solubility Methods of Estimation for Organic Compounds*; Marcel Dekker: New York, 1992.

$$c_{ppm} = S_w \times MW \times 10^3 \quad (14a)$$

$$\log(c_{ppm}) = -\log P + 3.8 + \log(MW) \quad (14b)$$

OI−17(8═9)−CCN as 4.8 ppm at 21 °C, which from (14b) suggests that log $P = 5.664$.

Since there is little data on log $P$ for other OI compounds, we need a method to estimate log $P$. A widely used procedure is $C$ log $P$.[23] However it is well-known that $C$ log $P$ over estimates the partition coefficient of strongly hydrophobic compounds.[22] Thus for OI−17(8═9)−CCN, $C$ log $P = 7.947$ which is 2.283 too high. Since our interest is in strongly hydrophobic compounds, we will assume

$$\log P = C \log P - 2.283 \quad (14c)$$

Using (14c) we evaluated log $P$ for the various molecules (see Table 2). The results are plotted vs the observed corrosion efficiencies in Figure 8. Clearly there is a correlation, with an optimum corrosion inhibition efficiency at log $P \approx 5$.

In refs 3 and 12 the corrosion inhibition rates were determined in experiments using 10 ppm of OI in water. However, as shown by McMahon,[7] the solubility of these compounds may be less than 10 ppm. Using (14b), Figure 9 shows the concentration of the inhibitor in water as a function of log $P$ (assuming that 10 ppm was added). When the amount of inhibitor exceeds its solubility in water, the extra inhibitor forms a separate phase in the system (a miscelle phase for the case of OI compounds). Since the amount of inhibitor is small compared to that of water, we assume that formation of an OI monolayer on the metal surface occurs from the water phase. The concentration $c$ in units of mol cm$^{-3}$ is the appropriate measure for transport of inhibitor to the surface and adsorption equilibrium. This concentration is related to the $c_{ppm}$ by (15)

$$c = \frac{c_{ppm} \times 10^{-6}}{MW} \quad (15)$$

**4.2 Langmuir Adsorption of Inhibitor.** The fraction of surface sites occupied by an inhibitor molecule can be written as

$$\theta_{eq} = \frac{Kc}{1 + Kc} \quad (16)$$

where $K$ is the Langmuir equilibrium constant and $c$ is the concentration. McMahon[7] found results well fitted by (16) for the adsorption of OI−17(8═9)−CCN on iron powder from solutions of OI in maltene and xylene. In addition, the saturation of corrosion inhibition with increasing concentration has been observed[3,8,21] to be similar to the saturation observed from solutions of OI in maltene and xylene.

For various OI we predicted the $K$ in (17) using $E_{coh}$ calculated from the MS FF,

$$K = r \exp\left(\frac{-\Delta S_{RIS}}{R}\right) \exp\left(\frac{E_{coh}}{RT}\right) \quad (17)$$

We find that $r = 42719$ cm$^3$/mol leads to a best fit with experiment.[3,8,12,21]

**4.3 Diffusive Formation of Monolayer.** The transport rate of matter from a uniform semiinfinite medium with initial concentration $c$ to a surface is given by[24] (18)

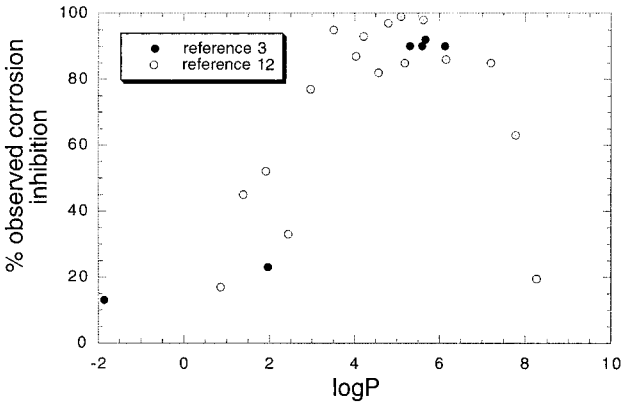


**Figure 8.** Comparison of observed corrosion inhibition with computed log $P$ values for a number of OI. The data are from refs 3 and 12.

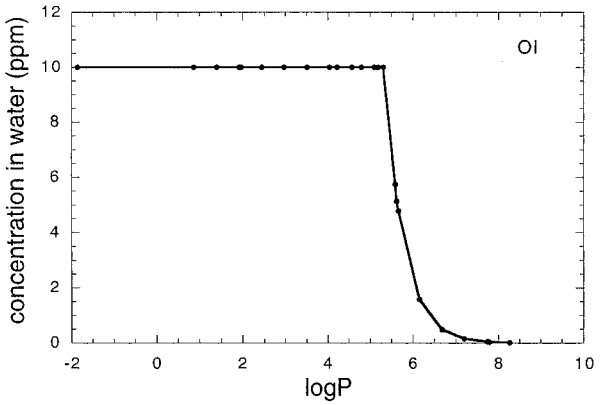


**Figure 9.** Predicted concentration of OI in the water phase upon adding 10 ppm of inhibitor. Equations 14b and 14c were used.

$$q = \frac{\sqrt{D}c}{(\sqrt{\pi}t)} \quad (18)$$

where $q$ is the mass flux to the surface, $D$ is the diffusion coefficient, $c$ is the concentration, and $t$ is the time. Here we assume that the surface immediately absorbs the inhibitor.

The total amount of inhibitor $Q(T)$ transported to the surface from time 0 to $T$ is given by

$$Q(T) = c\sqrt{\frac{DT}{\pi}} \quad (19a)$$

Thus the time $T_m$ to deliver an amount of inhibitor $Q_m$, sufficient for full monolayer coverage (1 molecule/66 Å$^2$), is given by (19b)

$$T_m = \frac{Q_m^2 \pi}{Dc^2} \quad (19b)$$

We write this as

$$T_m(h) = \frac{\tau}{c^2} \quad (19c)$$

where $\tau = 9.101 \times 10^{-19}$ h·cm$^6$/mol$^2$ leads to a best fit with experiment.

Because of the equilibrium (16), the surface has less than complete coverage, leading to a shorter time, $T_{cov}$, to form the equilibrium monolayer.

(23) Leo, A. J. *Chem. Rev.* **1993**, *93*, 1281.

(24) Bird, R.; Stewart, W. W.; Lightfoot, E. N. *Transport Phenomena*; John Wiley and Sons: New York, 1960.

(25) Jasinski, R. J. In *Surfaces, Inhibition and Passivation*; McCafferty, E., Brodd, R. J., Eds.; Electrochemical Society: Pennington, NJ, 1986; (Corrosion of Low-Alloy Steel in Cruce Oil/Brine/$CO_2$ Mixtures) p 139.

$$T_{cov} = \theta_{eq}^{\ 2}\, T_m \tag{20}$$

Neglecting desorption, the site coverage of the surface for $t < T_{cov}$ is given by (21), where $\theta$ is the fractional occupation

$$\theta(t) = \frac{\sqrt{t}}{\sqrt{T_m}} \text{ for } t < T_{cov} \tag{21}$$

on the surface binding sites ($\theta = 1$ for a monolayer with $\sigma = {}^1/_3$). Experiments[8,21] have clearly documented such transient behavior during corrosion experiments involving OI−17(8═9)−CCN, OI−17(8═9)−CCO, and OI−2−CCO.

The experiments[3,12] measuring the corrosion inhibition of the imidazoline compounds have been carried out in water. The solubility is extremely low in water but very little material is required on the surface. Thus for OI−17(8═9)−CCN just[7] 0.08 $\mu$g/cm$^2$ covers the (001) plane of $\alpha$-$Fe_2O_3$ (at a Fe site coverage of $\sigma = {}^1/_3$).

**4.4 Role of log *P* on the Rate of Forming a Monolayer.** Equation 14b implies that log(*P*/MW) > 2.8 leads to $c < 10$ ppm, even though 10 ppm was put into the solution. Since a typical OI has MW ≈ 316, this suggests that log *P* > 5.3 leads to reduced concentration. Assuming that all OI have the same diffusion constant, then (15) and (19c) lead to (22), where $T_m$ is transport time in h.

$$\log(T_m) = 2 \log P - 13.641 \text{ for } \log \frac{P}{MW} > 2.8 \tag{22a}$$

$$\log(T_m) = 2 \log (MW) - 8.041 \text{ for } \log \frac{P}{MW} \le 2.8 \tag{22b}$$

Thus for $c = 10$ ppm of OI−15−CCN (log $P = 5.07$, MW = 323.56; log(*P*/MW) = 2.56), we expect

$$T_{cov} = 0.000\ 95 \text{ h} = 3.4 \text{ s}$$

Equation 22 indicates that the transportation time for the inhibitor to form a monolayer changes dramatically with log *P*. This predicted time $T_m$ is presented in Figure 10 for OI−*n*−CCN as a function of *n*. Thus the time to transport the OI to the surface is expected to increase from 2.7 min for OI−17−CCN (log $P = 6.1$) to 5.9 h for OI−19−CCN (log $P = 7.2$) to 771.1 h (32 days) for OI−21−CCN (log $P = 8.3$).

Typically corrosion inhibition is measured by weight loss in experiments with durations of $T_{exp} = 24$−72 h.[12,24] Equation 22a implies that inhibitors with log $P > 7.7$ will still be adsorbing on the surface after 72 h. As discussed below, this explains the dramatic drop in CIE above $N = 19$ (Figure 7).

**4.5 Quantitative Predictions of the SAM Model.** In the SAM model, irreversible inhibitor transport occurs from water to the pore adjacent to the iron oxide surface. This transport occurs until the water phase holds sufficient inhibitor to be in equilibrium with the surface (in accordance with Langmuir adsorption in an oil rich phase). Equation 21 describes the surface coverage with time in the transient stage. Equations 16 and 17 describe the surface coverage at equilibrium. Equation 18 describes the diffusion time for forming a monolayer. We will integrate these equations to obtain the CIE, including the corrosion occurring while the system attains equilibrium.

We write the total corrosion without inhibitor as

$$C_{noinh} = kT_{exp} \tag{23}$$

where $T_{exp}$ is the total time for the experiment. Taking into account the fractional area (7) and assuming $T_{exp} > T_{cov}$, the total corrosion with inhibitor becomes

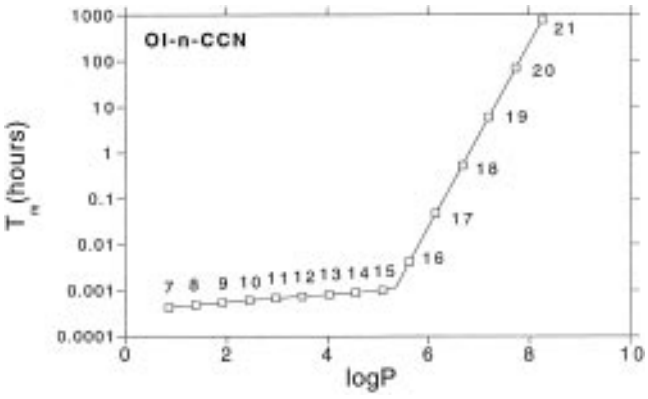


**Figure 10.** Predicted values of $T_m$, the time to transport a monolayer of OI to the surface. The dependence on log *P* and alkyl chain length is shown.

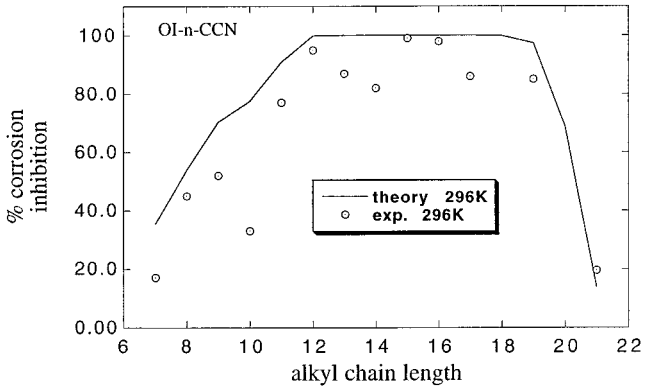


**Figure 11.** Corrosion inhibition for OI−*n*−CCN. Experimental values[11] are circles; predicted values are lines.

$$\frac{C_{inh}}{k} = \int_0^{T_{cov}} [1 - \theta(t)f]\, dt + \int_{T_{cov}}^{T_{exp}} (1 - \theta_{eq} f)\, dt$$

$$= T_{cov} - \frac{2}{3} f \frac{T_{cov}^{3/2}}{\sqrt{T_m}} + (T_{exp} - T_{cov})[1 - \theta_{eq} f] \tag{24}$$

where we used (21). Using (23) and (24), this leads to

$$\frac{C_{inh}}{C_{noinhv}} = 1 - \theta_{eq} f + \frac{1}{3}\theta_{eq}^{\ 3} f \frac{T_m}{T_{exp}} \tag{25}$$

Thus, the percentage CIE is given by

$$CIE = 100\left(1 - \frac{C_{inh}}{C_{ninh}}\right) \tag{26a}$$

$$= 100\theta_{eq} f\left(1 - \frac{1}{3}\theta_{eq}^{\ 2} \frac{T_m}{T_{exp}}\right) \tag{26b}$$

For $T_{exp} < T_{cov}$ we obtain

$$\frac{C_{inh}}{k} = T_{exp} - \frac{2}{3} f \frac{T_{exp}^{3/2}}{\sqrt{T_m}} \tag{26c}$$

and hence

$$\frac{C_{inh}}{C_{noinh}} = 1 - \frac{2}{3} f \sqrt{\frac{T_{exp}}{T_m}} \tag{26d}$$

or

$$\mathrm{CIE} = 100\left\{\frac{2}{3}f\sqrt{\frac{T_{\mathrm{exp}}}{T_{\mathrm{m}}}}\right\} \qquad (26e)$$

Equations 26b and 26e define the CIE in terms of $\theta_{eq}$, $f$, and $T_m$ (including the corrosion occurring while the system attains equilibrium). Thus the CIE can be calculated directly from the SAM model using (7), (16), (17), (22), and (26). We see that for systems with large log $P$, the experimental time $T_{exp}$ can play a dominant role. We have assumed that $T_{exp} = 72$ h in comparing various experiments, but $T_{exp}$ is not always well documented which may account for some disagreement between theory and experiment.[3,12]

For OI−$n$−CCN Figure 11 compares the predicted and experimental CIE at 296 K. The overall agreement is excellent. The theory explains that the decrease in CIE for $n < 12$ is due to $f < 1$ and hence indicates incomplete coverage of the surface. The decrease for $n > 19$ is due to slow transport to the surface (high log $P$). This suggests that more effective corrosion inhibitors for $n > 19$ could be designed by modifying the tails or pendant groups to be more soluble in water (e.g., by replacing $CH_2$ with an ether O).

The predicted temperature dependence of the corrosion inhibition is shown in Figure 12 for OI−$n$−CCN. This suggests that longer tails will have better high-temperature performance if the log $P$ is kept sufficiently low (below 7). We do not know of experimental data on the temperature dependence of corrosion inhibition for those systems.

The predictions of the SAM model is compared with available experimental results in Figure 13. In this figure we used the predicted log $P$ to disperse the results along the abscissica. We see that the SAM model agrees reasonably well with the maximum CIE.

## 5.0 Discussion

Atomistic modeling suggests the SAM model for corrosion inhibition by OI. The key elements of this model are (i) strong bonding by the imidazoline head group to the Fe site of $Fe_2O_3$ surface; (ii) self-assembly of the head groups to form a dense ordered overlayer; (iii) self-assembly of the hydrophobic tails to form a dense tightly-packed hydrophobic layer that blocks oxidation by serving as a barrier to diffusion of $H_2O$, oxygen, and electrons; and (iv) sufficient solubility and rate of transport of the inhibitor to the surface, implying that the SAM can be formed in a time fast compared to corrosion. Using the SAM model, all quantities affecting CIE ($E_{coh}$, $\Delta S$, log $P$, and $f$) can be evaluated purely from theory. This allows quantitative predictions to be made prior to experiment for how changes in the OI should affect the CIE. In addition, various specific predictions from the SAM model (e.g., the time for monolayer formation and the changes in solubility with log $P$) can be tested experimentally. This should lead to refinements and improvements in the SAM model. Thus the SAM model should be useful both for designing new experimental tests and for suggesting new classes of CI.

The SAM model is consistent with current experiments but is by no means proved. Thus we have discussed here only the most stable surface of $Fe_2O_3$. Clearly there will be other surfaces present and defects (steps, kinks, and defects) that might prefer differently-shaped inhibitors. The best CI formulation may include a blend of species suitable for such defect sites. In addition, other species (e.g., scale inhibitors) may be present that would compete with the OI for surface sites but which may not block corrosion. Furthermore, there are many other issues about what happens under flow conditions, where turbulence or cavitation may damage the protective layer. All these issues demand further study. However, the SAM model provides guidance that should be useful in designing future theoretical and experimental studies.

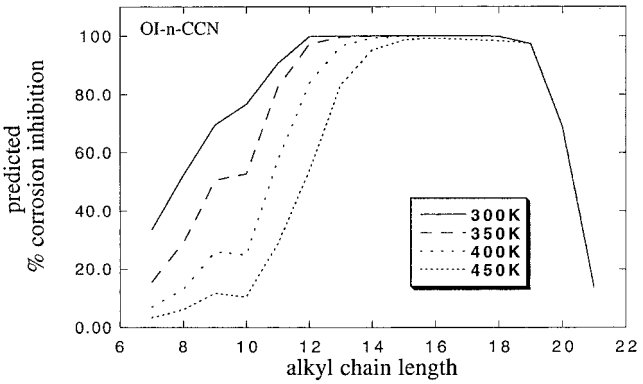


**Figure 12.** Predicted corrosion inhibition for OI−$n$−CCN as a function of temperature.

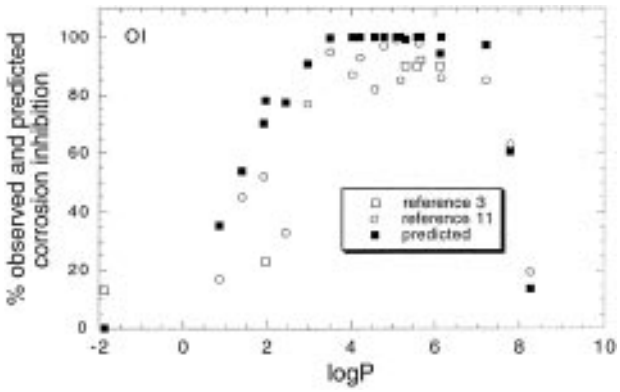


**Figure 13.** Observed and predicted corrosion inhibition of OI.

**Acknowledgment.** The research was funded by Chevron Petroleum Technology Co. (R. Heming), by DOE-BCTR (D. Boron), and by NSF-GCAG (Grant ASC 92-17368, R. Hildebrand). The facilities of the MSC are also supported by grants from NSF-CHE (Grant 95-22179), Aramco, Asahi Chemical, Chevron Chemical Co., Asahi Glass, Owens-Corning, Hercules, BP Chemical, Chevron Research and Technology Co., Avery-Dennison, and Beckman Institute. Calculations for this project were carried out on the Illinois NSF Supercomputer Center (L. Smarr) and on the JPL Cray (P. Messina).

LA960646Y